J Mater Sci (2010) 45:1361–1365
DOI 10.1007/s10853-009-4092-5

Investigation on preparation of nano-size $Gd_{0.2}Ce_{0.8}O_{2-\delta}$ material and its humidity sensing properties

Yu Wen Hao · Jing Wang · Zhou Ye Chen

Received: 6 September 2009 / Accepted: 25 November 2009 / Published online: 11 December 2009

Abstract The mixed-conductive ceramic oxide $Gd_{0.2}Ce_{0.8}O_{2-\delta}$ (GCO) particles with 40–50 nm were synthesized by using a combined citrate and EDTA complexation method. The material was characterized with powder X-ray diffraction, transmission electron microscopy, energy dispersive spectrometry, and X-ray photoelectron spectroscopy. A humidity sensor was fabricated by screening GCO onto a ceramic substrate with a pair of interdigitated electrodes. The sensor shows a linear relationship between logarithm impedance and relative humidity in the range of 33–98% when the measurement frequency range is 20 Hz–1 kHz. Typical response and recovery times of the sensor are 40 and 210 s, respectively, indicating that desorption rate of water molecule inside the GCO material is slower than the adsorption rate. The humidity sensing mechanism was discussed.

Introduction

The humidity sensor has been widely used in many automation systems. It is well known that a good humidity sensor should be focus on the improvement of following requirements, such as linear response, high sensitivity, short response time, and long-term stability.

Materials with these qualities, such as polymers, ceramics, and composites, have been studied and some of them showed their advantages in humidity applications [1–3]. Particularly, ceramic humidity sensors based on porous and sintered oxides have attracted much attention due to their chemical and physical stability [4, 5], high mechanical strength, and wide range of operation temperature. The previous reports on ceramic materials for humidity sensors mainly involved TiO_2 [6–8], ZrO_2 [9], ZnO [10, 11], perovskite oxides [12, 13], and so on.

Recently, more and more researchers pay their attention to exploitation of new nano-sized materials so as to obtain humidity sensors with excellent characteristics [14–16]. Gd-doped CeO_2 ceramic material with nano-size, which was proven to be the mixed ionic/electronic conductors, has drawn increasing attention in the field of electrochemistry due to its superior ionic conductivities being higher than those of the stabilized zirconia [17, 18] and the stability at reducing atmosphere being better than those of the perovskite-related oxides [19]. As we know, Gd-doped CeO_2 ceramic material has been used almost exclusively as the anode and electrolyte materials for solid oxide fuel cells [20, 21].

It was reported that the humidity sensing property improved with the increase of ionic and/or electronic conducting ability of the materials [22]. In this report, nano-sized $Gd_{0.2}Ce_{0.8}O_{2-\delta}$ (GCO) material was used to fabricate humidity sensor. The preparation, characterization, and humidity sensing properties of GCO material were investigated in detail. The sensing mechanism of GCO material was briefly discussed.

Experimental

Preparation and characterization of $Gd_{0.2}Ce_{0.8}O_{2-\delta}$ ceramic powders

$Gd_{0.2}Ce_{0.8}O_{2-\delta}$ ceramic powders were synthesized by a combined citrate and ethylene diamine tetraacetic acid

Y. W. Hao · J. Wang (✉) · Z. Y. Chen
School of Electronic and Information Engineering, Dalian University of Technology, 116023 Dalian, China
e-mail: wangjing@dlut.edu.cn

(EDTA) complexation method. In this method, stoichiometric amount of metal nitrate salts of $Gd(NO_3)_3{\cdot}6H_2O$ (>99.0%) and $Ce(NO_3)_3{\cdot}6H_2O$ (>99.0%) by 1:4 molar ratio were dissolved in an EDTA–citric acid aqueous solution with stirring at 70 °C. The molar ratio of metal ions:EDTA:citric acid was 1:1:1 in this batch. Ammonia was added to the mixture. Gelation occurred while the solution was concentrated at approximately 70 °C. The resulting metal–organic gels underwent pyrolysis and finally combustion, leaving metal oxide powders. The powder was calcined under air at 800 °C for 3 h in a furnace. The sample obtained in this way was denoted as GCO.

Powder X-ray diffraction (XRD) pattern was recorded with a Rigaku D/Max-2500 diffractometer (Japan) employing Cu K_α radiation ($\lambda = 0.1542$ nm) in the 2θ range of 5–70° with a scanning step of 5°/min at 40 kV and 200 mA. X-ray photoelectron spectroscopy (XPS) measurement was carried out on a VG ESCALAB MK2 spectrometer (England) by using an Al K_α ($h\upsilon = 1486.6$ eV) radioactivity source and operating at 12.5 kV and 250 W. The binding energy was calibrated against the C1s signal (284.6 eV) as a reference. The morphology of the sample was determined by a transmission electron microscopy (TEM) using a Philips Fei Tecnai Sprit apparatus operated at 120 kV. Energy dispersive X-ray spectroscopy (EDS) analysis of the sample was obtained on a Quanta 200F field-emission scanning electron microanalyser (Netherlands), employing the accelerating voltage of 120 kV. Sample was placed on the copper grid using highly conductive carbon paint as adhesive to fix the sample.

Sensor fabrication

The GCO power was ground with deionized water to form a paste, which was then screened onto the ceramic substrate with interdigitated electrodes. The thickness of the GCO film was 0.5 mm, and the area of the films was 8 mm × 4 mm. The humidity sensing film of the GCO material was dried at 200 °C in air for about 1 h.

Sensor measurement

Impedance measurements were carried out in a frequency range of 20 to 10^5 Hz at various relative humidities (RH). The equipment for the measurement is a ZL5 intelligent LCR test meter (Shanghai, China). The measurement of humidity was done at room temperature and RH levels were obtained by the saturated salt solution. The response and recovery times were determined over saturated salt solution of K_2SO_4 for 98% RH and $MgCl_2{\cdot}6H_2O$ for 33% RH in their equilibrium states [23], in which the gas was switched by manual within 0.5 s. The large round-bottomed chamber and narrow necked cap prevented the momentary perturbation of the humidity equilibrium.

Results and discussions

Structure characterization of GCO sample

Figure 1 shows XRD pattern of GCO sample. The XRD pattern clearly shows that the sample is single phase and all the reflection can be attributed to the cubic fluorite type structure. According to XRD data, the lattice parameter was calculated to be 0.5431 nm, which is higher than a lattice parameter of 0.54134 nm for pure CeO_2 (JCPDS 43-1002). This indicates that some places of Ce in the lattice are substituted by Gd atoms and a solid solution of Gd and Ce is formed. And the increase of the lattice parameter is believed to be caused by a larger atomic radius of Gd. In addition, according to Scherrer's semi-empirical formula, the crystallite size of GCO was calculated to be approximately 40 nm.

A typical TEM image of GCO sample is shown in Fig. 2, from which the average grain size of particles is measured to be approximately 40–50 nm. This is in good agreement with the XRD results. And it is obvious that the aggregation of the particles can be observed.

Figure 3 shows the spectrum of EDS analysis for the GCO. EDS analysis confirms that GCO composite material only consists Gd, Ce, and oxygen, and the atomic ratio of Gd/Ce is very close to the stoichiometry of based on the calculation of peak areas (see inserted Table). The strong Cu and C peak should be attributed to sample holder. Apart from that no other element peaks could be detected.

The results of XPS analysis of GCO sample are shown in Fig. 4, and Fig. 4a and b are for Ce 3d and Gd 4d,

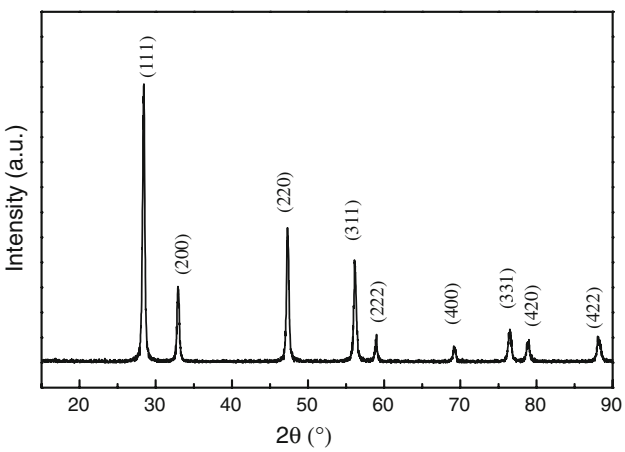

Fig. 1 XRD pattern of $Cd_{0.2}Ce_{0.8}O_{2-\delta}$ sample

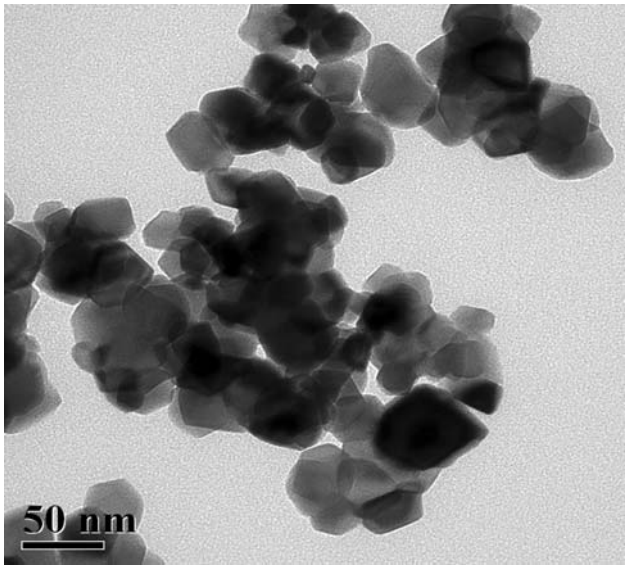

Fig. 2 TEM image of nanometer GCO material

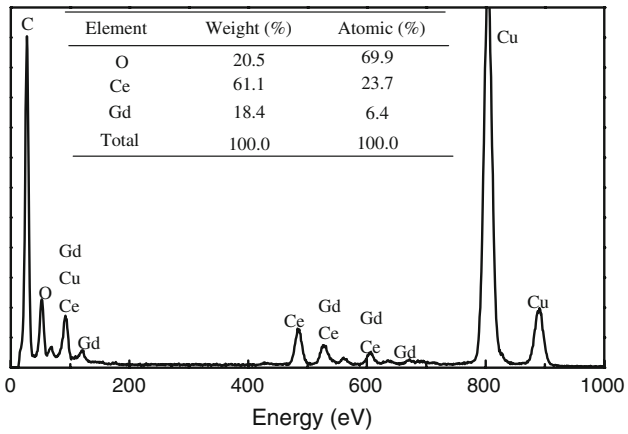

Fig. 3 EDS spectrum of $Gd_{0.2}Ce_{0.8}O_{2-\delta}$

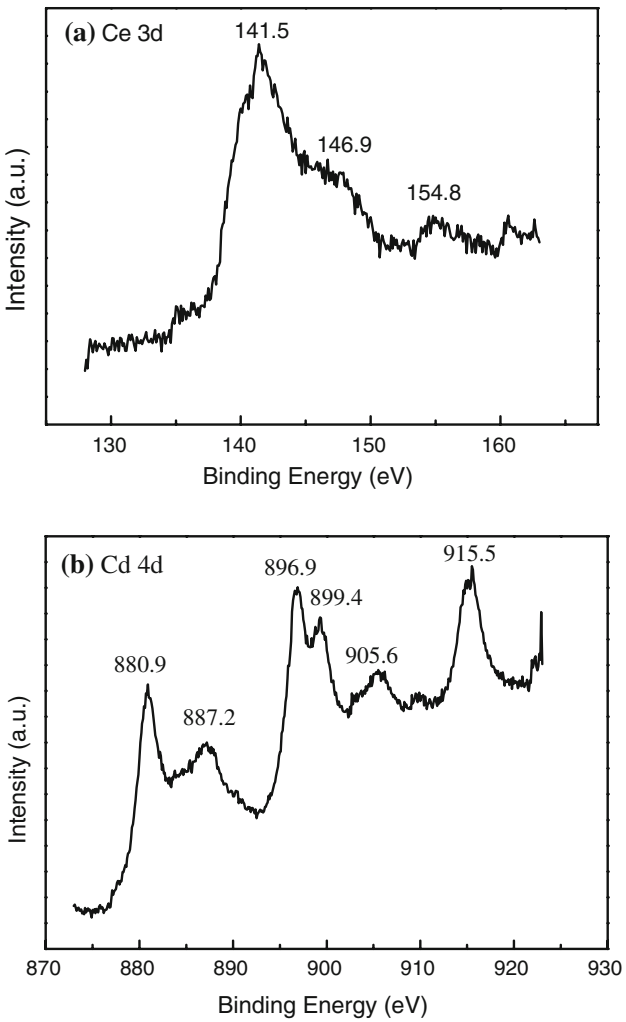

Fig. 4 XPS spectrum of Ce 3d (**a**) and Gd 4d (**b**) from surface region of GCO sample

respectively. Typically, the XPS spectrum of Ce 3d exhibits three distinct regions of envelopes, which is in good agreement with the reported results from the literature [24] (around 880–890 eV, 895–910 eV, and about 916 eV). The peak at approximately 916 eV is normally used as the spectroscopic marker to detect the presence of the Ce^{4+} state. According to the literature [25], it can be found that the peaks at 887.2 and 899.4 eV are assigned to Ce^{3+} state, indicating that Ce^{4+} and Ce^{3+} are co-existed on the surface of GCO sample. In addition, Gd $4d_{3/2}$ and Gd $4d_{5/2}$ peaks can be identified in Fig. 4b, which are located at 146.9 and 141.6 eV, respectively [26], indicating that Gd is present in Gd^{3+} of its characteristic chemical state. The existence of Ce^{4+} and Gd^{3+} in the surface region of GCO sample shows that the formation of oxygen vacancies is possible during the preparation of GCO material.

Humidity sensing properties of GCO sample

Figure 5 shows the plot of impedance of the sensor versus RH as function of measurement frequency at a voltage of 1 V. It can be found that the frequency obviously influence the humidity dependence of the impedance of the GCO sensor. Good logarithmic linearity in 30–98% RH range is obtained in the low frequency region such as 20 Hz–1 kHz. The impedance changes five orders of magnitude when RH varies from 30 to 98% RH. At low RH, the impedance decreased remarkably with increasing frequency, and the impedance difference between two measurement frequencies became progressively smaller with increasing RH.

The response and recovery behavior is an important property for the humidity sensors. Figure 6 shows the response and recovery characteristic of the GCO humidity sensor, measured at room temperature and 20 Hz. The response and recovery times are defined as the time required to reach the 90% of the final equilibrium signal.

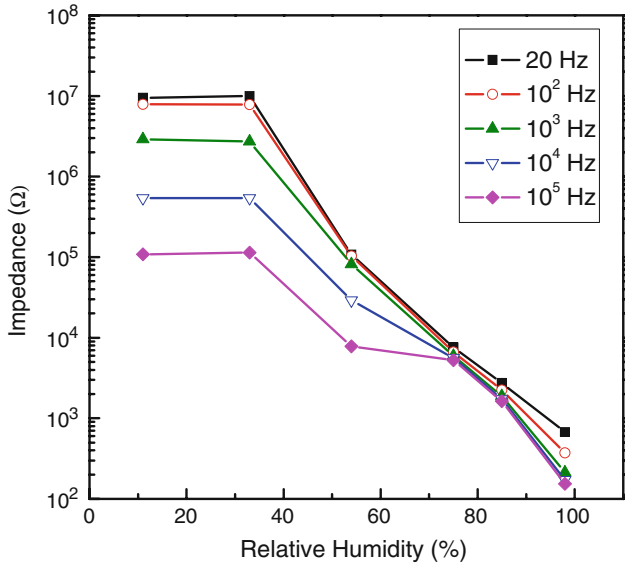

Fig. 5 Impedance versus relative humidity plot of GCO sensor at various frequencies

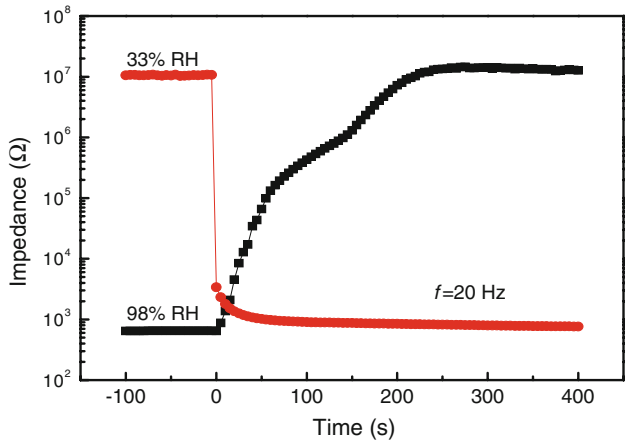

Fig. 6 Response and recovery properties of the GCO sample

The response time (as humidity changes from 33 to 98% RH) is about 40 s. The recovery time (from 98 to 33% RH) is about 210 s, which is longer than the response time. This phenomenon could be due to the slow desorption rate of water molecule inside the GCO material.

Figure 7 represents reversibility of resistance with variations in RH. Curve 'a' represents the change of resistance when the humidity increases, and curve 'b' for the decrease of the humidity. It is obvious that GCO material exhibits a narrow hysteresis, indicating that adsorption and desorption of GCO material are similar and the rate of desiccation of the adsorbed water is the same as that of the humidification.

Conductivity of ceramic and nanometer sensing materials varies with the amount of water adsorbed on the surface of them [27]. Unlike SiO_2 [28] and other porous

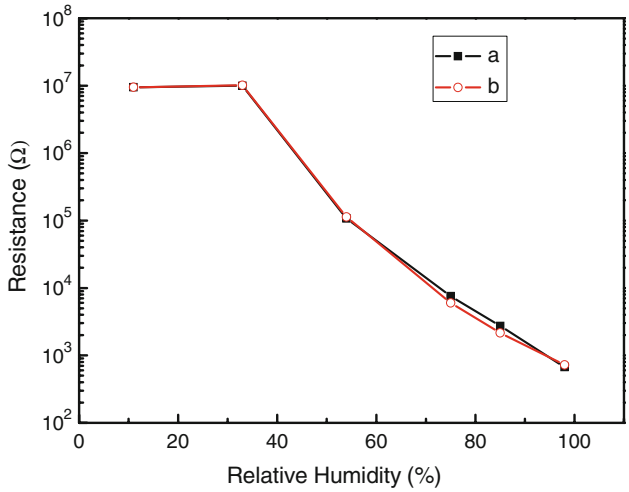

Fig. 7 Hysteresis property of GCO humidity sensor

oxides, for GCO material calcined at 800 °C for 3 h, hydroxyl groups on the surface are scarce and difficult to be originated. However, according to the literature [29], it was known that the presence of surface defect and oxygen vacancies could originate the proton when the water molecule was absorbed on the surface. The XPS data showed that the existence of Ce^{4+} and Gd^{3+} in the surface region of the GCO sample could imply the presence of oxygen vacancies. At low RH range, H_2O molecular was chemisorbed on the surface of GCO material. And the adsorption of vapor H_2O molecular on oxygen vacancies ($V_O^{\bullet\bullet}$) and lattice oxygen (O_O^x) can lead to the formation of an interstitial proton ($OH_i^{\bullet}$) associating strongly with a neighbor O_O^x according to the following equation:

$$H_2O(g) + V_O^{\bullet\bullet} + O_O^x \Leftrightarrow 2OH_i^{\bullet}.$$

The interstitial proton ($OH_i^{\bullet}$) may hop around the oxygen vacancies ($V_O^{\bullet\bullet}$). Thus, at low RH, dominating conduction process is proton hopping. As RH increases, liquid water molecular is abundant on the surface of GCO material, and a large amount of H^+ ions dissociated from the adsorbed water become the dominant charged carries [30], for which the transport mechanism is assured by H^+ transfer between adjacent water molecules [31]. As a superior ionic conductor, the ionic conductivity of GCO is significantly enhanced at higher RH because H^+ transport is more energetically favorable than the proton hopping. This may explain the reason that the resistance decreases rapidly with increasing RH as shown in Fig. 5.

Conclusion

Nano-sized GCO powders were synthesized via citrate and EDTA complexation method. The sensor prepared with

GCO powders showed that electrical impedance behavior dependent on the RH. And the sensor exhibited a logarithmic linear response of RH over the range of 33–98% in the range of 20 Hz–1 kHz. Typical response and recovery times of the sensor are 40 and 210 s, respectively. From the results, it could be proposed that, at low RH, the interstitial proton ($OH_i^{\bullet}$) hopping around the oxygen vacancies is dominant conduction process. At high RH, the transport mechanism is assured by H^+ transfer between adjacent adsorbed water molecules.

Acknowledgement We gratefully thank Mr. Peng Jun Yao for his help in the experiments.

References

1. Yamazoe N, Shimizu Y (1986) Sens Actuator 10:379
2. Li ZY, Zhang HN, Zheng W, Wang W, Huang HM, Wang C, MacDianmid AG, Wei Y (2008) J Am Chem Soc 130:5036
3. Traversa E (1995) Sens Actuator B 23:135
4. Timar-Horvath V, Juhasz L, Vass-Varnai A, Perlaky G (2008) Microsyst Technol 14:1081
5. Fagan JG, Amarakoon VR (1993) Am Soc Bull 72:119
6. Saha D, Giri R, Mistry KK, Sengupta K (2005) Sens Actuators B 107:323
7. Chow LLW, Yuen MMF, Chan PCH, Cheung AT (2001) Sens Actuators B 76:310
8. Wu RJ, Sun YL, Lin CC, Chen HW, Chavali M (2006) Sens Actuators B 115:198
9. Wang J, Su MY, Qi JQ, Chang LQ (2009) Sens Actuator B 139:418
10. Zhang YS, Yu K, Ouyang SX, Luo LQ, Hu HM, Zhang QX, Zhu ZQ (2005) Physica B 368:94
11. Wang XH, Ding YF, Zhang J, Zhu ZQ, You SZ, Chen SQ, Zhu JZ (2006) Sens Actuators B 115:421
12. Wang J, Xu BK, Liu GF, Zhang JC, Zhang T (2000) Sens Actuators B 66:159
13. Yuk J, Troczynski T (2003) Sens Actuators B 94:290
14. Leung YP, Choy WCH, Yuk TL (2008) Chem Phys Lett 457:198
15. Wang ZY, Chen C, Zhang T, Guo HL, Zou B, Wang R, Wu FQ (2007) Sens Actuators B 126:678
16. Yadav BC, Srivastava R, Dwivedi CD, Pramanik P (2008) Sens Actuators B 131:216
17. Kharton VV, Marques FMB, Atkinson A (2004) Solid State Ion 174:135
18. Shimonosono T, Hirata Y, Ehira Y, Sameshima S, Horita T, Yokokawa H (2004) Solid State Ion 174:27
19. Kharton VV, Kovalesky AV, Viskup AP, Shaula AL, Marques FMB (2003) Solid State Ion 160:247
20. Yin X, Hong L, Liu ZL (2006) Appl Catal A Gen 300:75
21. Park SH, Yoo HI (2009) Phys Chem Chem Phys 11:391
22. Hashmi SA (1997) Solid State Ion 96:209
23. Greenspan L (1977) J Res Natl Bureau Stand A 81:89
24. Datta P, Majewski P, Aldinger F (2009) Mater Charact 60:138
25. Praline G, Koel BE, Hange RL, Lee HI, White JM (1980) J Electron Spectrosc Relat Phenom 21:17
26. Uwamino Y, Ishizuka T, Yamatera H (1984) J Electron Spectros Relat Phenom 34:67
27. Kulwicki BM (1991) J Am Ceram Soc 74:697
28. Anderson JH, Parks GA (1968) J Phys Chem 78:3662
29. Song SJ, Washsman ED, Rhodes J, Dorris SE, Balachandran U (2004) Solid State Ion 167:99
30. Wang J, Wu FQ, Shi KH, Wang XH, Sun PP (2004) Sens Actuators B 99:586
31. Daia PM, Furtado CS, Ferreira AJ (2005) Sens Actuators B 107:353